Journal of Young Pharmacists, 2026; 18(2):450-456.
https://www.jyoungpharm.org

Original Article

Computational Identification of Aggregation-Prone Regions in Brain-Derived Neurotrophic Factor (BDNF)

Muthiah Ramanathan[1,*], Radhakrishnan Nithya[2]

[1]Department of Pharmacology, PSG College of Pharmacy, (Affiliated to The Tamil Nadu Dr. MGR Medical University, Chennai), Coimbatore, Tamil Nadu, INDIA.
[2]Department of Pharmaceutics, PSG College of Pharmacy, (Affiliated to The Tamil Nadu Dr. MGR Medical University, Chennai), Coimbatore, Tamil Nadu, INDIA.

ABSTRACT

Background: Brain-Derived Neurotrophic Factor (BDNF) is a promising therapeutic protein for neurological disorders; however, its clinical application is limited by aggregation susceptibility, which can compromise stability, efficacy, and safety. Identification of aggregation-prone structural determinants is therefore essential for rational stabilization strategies. **Materials and Methods:** The homodimeric structure of human BDNF (PDB ID: 1BND) was analyzed using the BioLuminate module of Schrödinger for residue-level structural interrogation and energetic decomposition. Aggregation propensity was evaluated using AggScore, Aggrescan, and Zyggregator algorithms. Residue-wise hydrophobic energetic contributions, stabilizing and destabilizing interaction energies, Solvent-Accessible Surface Area (SASA), and patch surface areas were quantified for 293 residues across both chains. Descriptive statistics, correlation analysis, and chain-wise comparisons were performed to identify dominant aggregation hotspots. **Results:** Aggregation scores demonstrated marked heterogeneity (mean 2.78±3.26; maximum 17.13), revealing a strongly right-skewed distribution dominated by isolated high-intensity hotspots. Chain A exhibited a prominent aggregation-prone cluster within residues 60-63, centered on GLY62, characterized by elevated aggregation score and increased solvent accessibility. Chain B displayed a broader but lower-intensity aggregation pattern, with consistent signatures observed in the C-terminal region (95-110). Global statistical analysis showed no significant linear correlation between hydrophobic energetic contribution and aggregation score, indicating that aggregation susceptibility is governed by multifactorial structural determinants rather than hydrophobicity alone. **Conclusion:** Aggregation propensity in BDNF appears to be concentrated within discrete structural microdomains. The identified hotspot provides a structural basis for rational protein engineering and formulation strategies to enhance therapeutic stability. Experimental validation is required to confirm these computational findings.

Keywords: AggScore, Brain-Derived Neurotrophic Factor, Computational Analysis, Hydrophobic Interactions, Protein Aggregation, Solvent Accessibility.

Correspondence:
Dr. Muthiah Ramanathan
Department of Pharmacology, PSG College of Pharmacy, Coimbatore, Tamil Nadu, INDIA.
Email: muthiah.in@gmail.com
ORCID: 0000-0002-2186-6554

Received: 21-02-2026;
Revised: 06-03-2026;
Accepted: 16-04-2026.

INTRODUCTION

Brain-Derived Neurotrophic Factor (BDNF) is a homodimeric member of the neurotrophin family that plays a fundamental role in neuronal differentiation, survival, synaptic plasticity, and long-term potentiation. Through activation of the Tropomyosin Receptor Kinase B (TrkB) receptor, BDNF orchestrates critical signaling cascades governing neurogenesis and synaptic remodeling (Colucci-D'Amato *et al*., 2020). Owing to its profound neuroprotective and neuroregenerative properties, recombinant BDNF has been investigated as a therapeutic candidate for a wide spectrum of neurological and psychiatric disorders, including Alzheimer's disease, Parkinson's disease, Huntington's disease, spinal cord injury, major depressive disorder, and ischemic brain injury.

Despite its compelling therapeutic potential, the development of BDNF as a protein-based biologic is severely constrained by intrinsic aggregation liability (Majid and Khan, 2023). Aggregation of protein therapeutics is a major pharmaceutical challenge, as it can compromise conformational integrity, reduce receptor-binding affinity, diminish biological potency, accelerate chemical degradation, and increase immunogenic risk. From a regulatory perspective, aggregated species are considered critical quality attributes due to their potential to trigger adverse immune responses (Pham and Meng, 2020). Therefore, identifying and mechanistically characterizing aggregation-prone determinants

OPEN ACCESS

Manuscript TECHNOMEDIA

DOI: 10.5530/jyp.20260049

Publishing Partner : Manuscript Technomedia. [www.mstechnomedia.com]

within BDNF is essential for enabling rational stabilization strategies.

Protein aggregation is a complex, multi-factorial phenomenon governed by structural, energetic, and physicochemical parameters (Rojekar *et al*., 2025). Key drivers include exposure of hydrophobic residues, aromatic π-π stacking interactions, β-sheet nucleation propensity, conformational flexibility of glycine-rich segments, electrostatic imbalance, and local energetic destabilization (Rabe *et al*., 2009). Importantly, aggregation propensity is rarely uniform across a protein structure; rather, it is typically dominated by discrete spatially clustered hotspots that function as nucleation centers.

While numerous computational tools exist to predict aggregation-prone regions, most studies rely on a single algorithm or sequence-based predictors alone (Navarro and Ventura, 2022). However, aggregation is inherently multidimensional, and robust mechanistic inference requires integration of structure-based scoring, intrinsic sequence propensity, solvent accessibility analysis, and energetic decomposition. A statistically supported, chain-resolved structural interrogation is therefore necessary to define aggregation-driving nuclei with high predictive confidence.

In this study, we perform an integrated computational dissection of aggregation determinants in BDNF at residue-level resolution. By combining structure-informed aggregation scoring, sequence-driven aggregation prediction, β-sheet aggregation modeling, solvent accessibility quantification, energetic contribution analysis, and statistical distribution profiling across 293 residue entries, we delineate dominant aggregation nuclei and establish a mechanistic hierarchy of aggregation drivers. This integrative framework provides actionable insights for rational protein engineering and formulation optimization of BDNF as a therapeutic biologic.

MATERIALS AND METHODS

Structural Dataset and Residue-Level Data Extraction

The biologically active homodimeric structure of human Brain-Derived Neurotrophic Factor (BDNF) (PDB ID: 1BND; resolution 2.30 Å) was retrieved from the Protein Data Bank. Structural preparation was performed using the Protein Preparation Wizard in BioLuminate (Schrödinger Release 2023-4, Schrödinger, LLC, New York, NY, USA). Preparation steps included bond order assignment, addition of hydrogen atoms, correction of formal charges, optimization of hydrogen-bonding networks, and restrained minimization using the OPLS4 force field with heavy-atom convergence criteria of 0.3 Å RMSD.

A total of 293 residue-level entries across Chain A and Chain B were analyzed. For each residue, quantitative descriptors including AggScore-based aggregation score, Solvent-Accessible Surface Area (SASA), relative side-chain solvent accessibility ratio, patch surface area, and energetic contributions (positive destabilizing, negative stabilizing, and hydrophobic components) were extracted using the BioLuminate residue interaction analysis module.

Multi-Algorithm Aggregation Prediction

Aggregation propensity was evaluated using three complementary computational frameworks to ensure multidimensional assessment of aggregation determinants. AggScore analysis was performed within the BioLuminate environment using default structural aggregation parameters. Aggregation-prone residues were defined as those exceeding the 75th percentile of the residue-level aggregation score distribution. Surface hydrophobic clustering thresholds and spatial exposure criteria were retained at software-defined default settings to preserve methodological consistency.

Intrinsic sequence-based aggregation propensity was assessed using the online Aggrescan server (version 2023). Predictions were conducted using default parameters, including a window size of five residues and the experimentally derived a3v intrinsic aggregation propensity scale. Residues exhibiting positive normalized aggregation propensity values were classified as aggregation-prone segments.

To further evaluate β-sheet-driven aggregation potential, Zyggregator analysis was performed using its standard physicochemical weighting framework, which integrates hydrophobicity, charge distribution, and secondary structure propensity. Default algorithm coefficients were applied without modification. Regions with aggregation probability scores exceeding the server-defined threshold were considered aggregation-susceptible.

The outputs from AggScore, Aggrescan, and Zyggregator were subsequently integrated by cross-referencing residue-level predictions across all three methods to identify concordant aggregation hotspots. This multi-algorithm approach enabled simultaneous evaluation of structure-dependent exposure, intrinsic sequence-encoded aggregation propensity, and β-sheet-mediated aggregation mechanisms.

Energetic Contributions and Solvent Accessibility Analysis

Residue-wise energetic decomposition was performed using the BioLuminate module (Schrödinger, LLC, New York, NY, USA) following structural preparation of the BDNF dimer (PDB ID: 1BND). The prepared structure was subjected to residue-level interaction energy analysis to quantify individual energetic contributions within the protein microenvironment. For each residue, total interaction energy was decomposed into stabilizing (negative) and destabilizing (positive) components based on intramolecular interaction profiles. Additionally, hydrophobic energetic contributions were calculated in kcal/mol to estimate

the extent of non-polar interactions contributing to local aggregation-driving forces. These energetic descriptors were extracted for all residues across both chains and incorporated into the statistical dataset.

Side-chain solvent accessibility was quantified using Solvent-Accessible Surface Area (SASA) calculations implemented within BioLuminate. Relative solvent accessibility ratios were computed by normalizing residue exposure against standard reference values for fully exposed amino acids (Tien *et al.*, 2013). This normalization enabled identification of residues with elevated surface exposure. Because aggregation requires intermolecular contact, solvent-exposed hydrophobic and aromatic residues were considered particularly relevant for aggregation susceptibility.

To evaluate spatial clustering of aggregation determinants, aggregation-prone residues were mapped onto the protein surface, and patch surface areas were calculated based on contiguous solvent-accessible regions exceeding aggregation score thresholds. Patch Area (Å²) was determined by summing the surface contributions of neighbouring residues within defined spatial proximity (Jones and Thornton, 1997). This approach enabled identification of extended aggregation-competent domains rather than isolated single-residue vulnerabilities.

All energetic, accessibility, and patch parameters were exported as residue-level quantitative descriptors and subjected to subsequent statistical analysis and chain-wise comparisons.

Statistical Analysis

All residue-level quantitative descriptors were statistically evaluated to characterize aggregation behavior within the BDNF dimer. Descriptive statistics including mean, Standard Deviation (SD), minimum, maximum, and percentile distributions were calculated for aggregation scores, hydrophobic energetic contributions, stabilizing and destabilizing interaction energies, solvent accessibility ratios, and patch surface areas. To assess inter-variable relationships, Pearson correlation analysis was performed between aggregation score and hydrophobic contribution, aggregation score and solvent accessibility, and hydrophobic contribution and solvent accessibility. Correlation strength was interpreted based on Pearson's correlation Coefficient (r), and linear regression analysis was conducted to quantify predictive relationships. Coefficient of Determination (R^2) values were calculated to assess the proportion of variance explained. Comparative analysis between Chain A and Chain B was conducted using unpaired two-tailed t-tests to determine statistical differences in aggregation score, hydrophobic contribution, and solvent accessibility. Statistical significance was defined at $p<0.05$. All analyses were performed using GraphPad Prism (version 10.0; GraphPad Software, USA). Results are expressed as mean±SD unless otherwise specified.

RESULTS

Aggregation Distribution and Statistical Characterization

The aggregation landscape of BDNF exhibits pronounced heterogeneity and statistical asymmetry (Table 1). Across 293 residues, the mean aggregation score was 2.78±3.26, with a maximum value of 17.13. The aggregation score distribution demonstrated strong positive skewness (skewness coefficient=2.20), and Shapiro-Wilk testing confirmed significant deviation from normality (W=0.681, $p<0.0001$). The marked disparity between the mean and maximum values quantitatively supports a nucleation-dominated aggregation pattern characterized by rare high-intensity hotspots rather than uniform structural instability.

Patch-level analysis further reinforced this heterogeneity. Sixty aggregation-associated surface patches were identified, exhibiting a mean surface area of 147.55±195.52 Å², with values ranging from 16.00 to 1039.80 Å². The patch size distribution demonstrated pronounced positive skewness (skewness coefficient=2.34), indicating the presence of rare but disproportionately large aggregation-competent domains. Shapiro-Wilk testing confirmed non-normal distribution of patch sizes (W=0.64, $p<0.0001$). Several extended patches exceeded 700 Å², suggesting that aggregation susceptibility is driven by clustered surface domains rather than isolated residue-level vulnerabilities.

Hydrophobic energetic contributions averaged 0.43±0.3 kcal/mol, with moderate dispersion across residues, whereas stabilizing (negative) energetic components demonstrated broader variability. This energetic heterogeneity suggests that local destabilization and hydrophobic clustering are unevenly distributed across the BDNF structure, reinforcing the concept that aggregation propensity is concentrated within discrete structural microenvironments.

Chain-wise Comparison of Aggregation and Energetic Parameters

Chain-wise analysis revealed differential aggregation behavior between the two monomeric subunits of BDNF. Residue-level aggregation scoring identified a dominant high-intensity hotspot in Chain A centered at GLY62, which exhibited the highest aggregation score (17.13) among all analyzed residues (Figure 1). This hotspot formed a contiguous cluster with PRO60, MET61, and TYR63, spanning residues 60-63. Collectively, these residues demonstrated elevated solvent accessibility and increased hydrophobic energetic contribution relative to neighboring regions. In addition, this segment displayed higher positive energetic contributions, indicative of localized destabilization consistent with aggregation-prone microdomains.

The elevated aggregation score at GLY62, together with the hydrophobic contribution of MET61 and the aromatic character

of TYR63, suggests that this segment represents a structurally vulnerable region within Chain A (Figure 2). The spatial clustering of aggregation-prone residues within this narrow sequence window supports the presence of a localized aggregation nucleus rather than diffuse structural instability. Statistical validation further confirmed the exceptional nature of this region: GLY62 exhibited a Z-score of 4.71 relative to the global aggregation score distribution, confirming its classification as an extreme statistical outlier. The mean aggregation score for Chain A was 2.94±4.08, whereas Chain B exhibited a mean of 2.01±2.57. Independent two-tailed *t*-test analysis revealed a statistically significant difference between the two chains (t=2.08, p=0.039), indicating modest but statistically significant differences in aggregation score distribution between the two chains.

In contrast, Chain B exhibited a broader but comparatively lower-intensity aggregation profile. Moderate aggregation scores were observed for aromatic residues such as PHE56 and TYR55, consistent with their potential involvement in hydrophobic and π-π interactions. Additionally, the C-terminal segment spanning residues 95-110 displayed aggregation signatures across multiple predictive frameworks, including β-sheet propensity models, suggesting a secondary aggregation-prone region that may contribute to aggregation propagation rather than primary nucleation.

Correlation between Energetic Contributions and Solvent Accessibility

Residues identified as high-intensity aggregation hotspots exhibited elevated hydrophobic energetic contributions alongside reduced stabilizing (negative) energy components when compared with the overall residue population. These residues also demonstrated increased solvent accessibility ratios, indicating enhanced surface exposure (Figure 3). Pearson correlation analysis demonstrated a statistically significant but very weak negative association between hydrophobic energetic contribution and aggregation score (r=-0.129, p=0.039; R^2=0.017). Although localized hotspot regions exhibited elevated hydrophobic contributions, the global residue-level dataset did not demonstrate

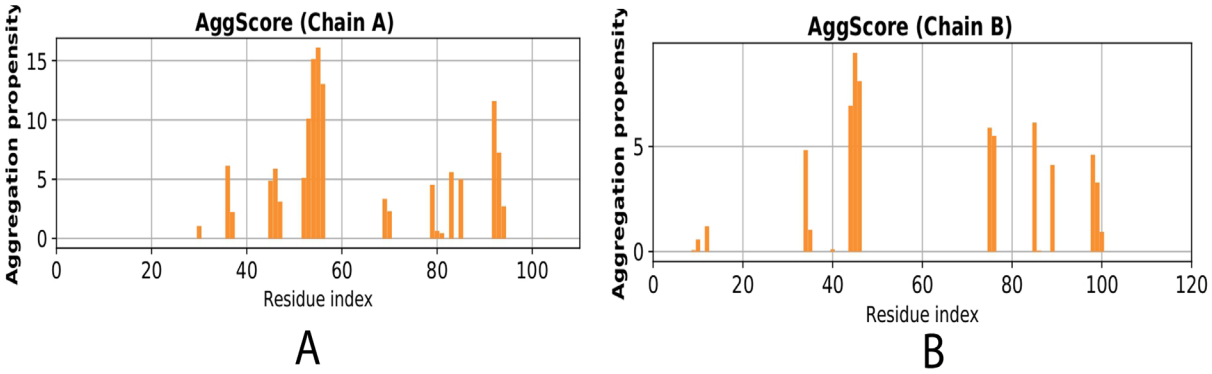

Figure 1: Residue-wise aggregation propensity profile of Brain-Derived Neurotrophic Factor (BDNF) based on AggScore analysis across 293 residues. (A) Chain A and (B) Chain B. Aggregation propensity is plotted as a function of residue index, demonstrating heterogeneous distribution with distinct high-intensity peaks, particularly within Chain A.

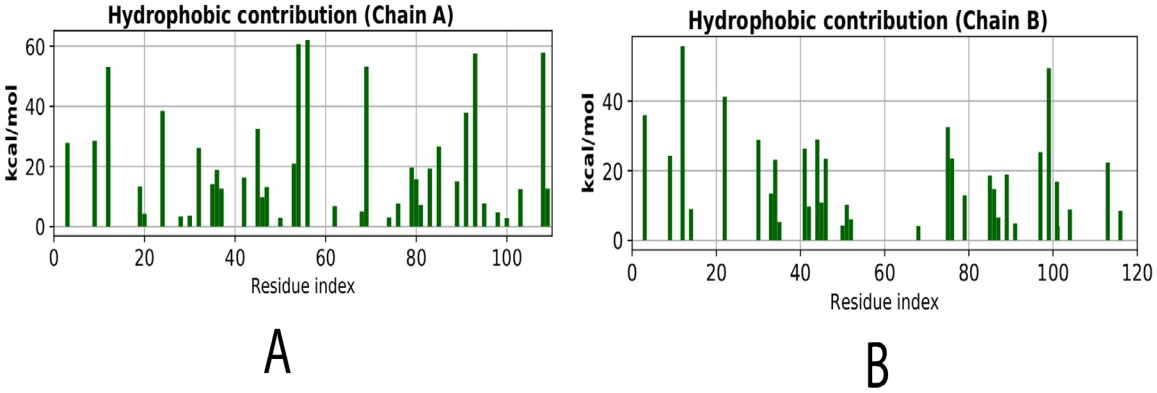

Figure 2: Residue-wise hydrophobic energetic contribution profile of Brain-Derived Neurotrophic Factor (BDNF) derived from residue-level energetic decomposition. (A) Chain A and (B) Chain B. Hydrophobic energetic contributions (kcal/mol) are plotted as a function of residue index, illustrating heterogeneous distribution across both monomeric subunits. Chain A demonstrates localized regions of elevated hydrophobic contribution corresponding to aggregation-prone segments, whereas Chain B exhibits broader but comparatively moderate hydrophobic distribution.

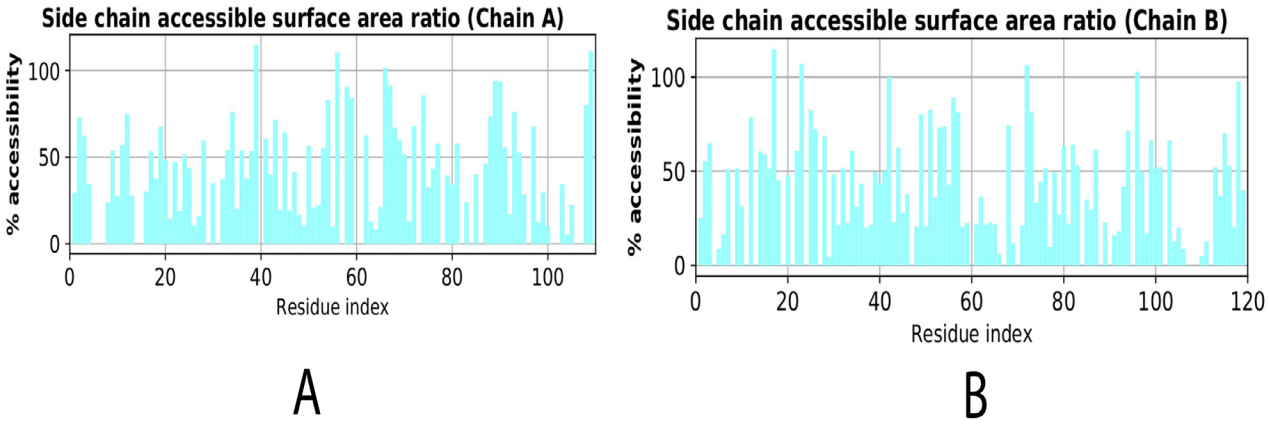

Figure 3: Residue-wise side-chain solvent accessibility profile of Brain-Derived Neurotrophic Factor (BDNF). (A) Chain A and (B) Chain B. Relative Solvent Accessibility (RSA) values, calculated from Solvent-Accessible Surface Area (SASA) and normalized against reference exposure values, are plotted as a function of residue index. Regions exhibiting elevated solvent accessibility correspond to surface-exposed residues that may facilitate intermolecular interactions and aggregation initiation.

Table 1: Descriptive Statistical Summary of Aggregation and Energetic Parameters.

Parameter	Mean±SD	Minimum	Maximum
Aggregation Score	2.78±3.26	0.28	17.13
Patch Surface Area (Å²)	147.55±195.52	16.00	1039.80
Hydrophobic Energy (kcal/mol)	0.43±0.3	0.00	1.53
Positive Energy Contribution	360.44±369.61	8.14	1268.31
Negative Energy Contribution	−0.65±0.77	−2.28	1.78
SASA (%)	29.39±19.25	1.00	60.00

a strong linear relationship, indicating that hydrophobicity alone is insufficient to predict aggregation propensity. This finding suggests that aggregation susceptibility is not driven solely by hydrophobic magnitude but is influenced by the combined effects of structural exposure, local energetic destabilization, and spatial clustering.

Notably, convergence of elevated aggregation score, increased solvent accessibility, and enhanced hydrophobic energetic contribution was observed within residue ranges 55-65 and 95-110. These segments consistently displayed higher aggregation-related parameters relative to surrounding regions, supporting their identification as dominant aggregation-prone domains within the BDNF structure.

DISCUSSION

The present integrated computational analysis indicates that aggregation susceptibility in BDNF is not uniformly distributed across the protein structure but is concentrated within specific residue clusters. Descriptive statistical analysis demonstrated a right-skewed distribution of aggregation scores, with a limited number of residues exhibiting markedly higher values than the overall mean. This observation suggests that aggregation propensity may be driven by localized high-intensity segments rather than generalized structural instability.

Chain-wise comparison revealed that Chain A contains a dominant aggregation hotspot within residues 60-63, particularly centered on GLY62. This region displayed the highest aggregation score along with increased hydrophobic energetic contribution and elevated solvent accessibility. The concurrence of these parameters suggests that this microdomain represents a structurally vulnerable segment prone to intermolecular association. The elevated hydrophobic contribution observed for MET61, together with the aromatic nature of TYR63 and the conformational characteristics of GLY62 and PRO60, may collectively enhance local aggregation susceptibility through surface exposure and hydrophobic interactions. Although glycine is intrinsically non-hydrophobic and does not directly promote hydrophobic aggregation, its conformational flexibility may facilitate transient structural fluctuations that expose adjacent hydrophobic residues such as MET61 and TYR63. Therefore, the aggregation propensity associated with GLY62 likely arises from its structural positioning within a flexible loop region rather than from intrinsic physicochemical aggregation potential. Structural mapping onto the BDNF crystal structure (PDB ID: 1BND) indicates that residues 60-63 are located within a loop region connecting β-strands. Loop regions are often associated with increased solvent exposure and structural mobility, which

may enhance aggregation susceptibility under destabilizing conditions.

In contrast, Chain B exhibited a broader but lower-intensity aggregation profile. Although moderate aggregation scores were observed in aromatic residues such as PHE56 and TYR55, (Elhassan *et al*., 2025). The absence of an extreme high-magnitude hotspot comparable to GLY62 suggests quantitative differences in hotspot intensity between the two chains; however, given the homodimeric symmetry of BDNF, functional asymmetry cannot be concluded without experimental validation. The C-terminal segment (residues 95-110), which showed aggregation signatures across predictive models, may contribute to aggregation propagation rather than primary nucleation.

Given that BDNF exists as a homodimer, the spatial positioning of aggregation-prone residues relative to the dimer interface may influence aggregation behavior. Preliminary structural mapping suggests that the 60-63 segment appears spatially positioned in proximity to the dimer interface based on structural visualization, which may contribute to the quantitative differences in aggregation score distribution observed between Chain A and Chain B. The correlation between hydrophobic energetic contribution and aggregation score further emphasizes the importance of hydrophobic clustering in BDNF aggregation. Although localized hydrophobic enrichment was observed within hotspot regions, global statistical analysis indicates that hydrophobicity alone does not account for aggregation susceptibility. Residues with elevated hydrophobic energy values and higher solvent accessibility were consistently associated with increased aggregation propensity (Malleshappa Gowder *et al*., 2014). These findings indicate that surface-exposed hydrophobic regions are likely to facilitate intermolecular contacts, promoting aggregation under destabilizing conditions.

From a pharmaceutical perspective, identification of discrete aggregation-prone segments provides opportunities for targeted stabilization strategies (Rahban *et al*., 2023). Site-directed modification of residues within the 60-63 region could potentially reduce aggregation susceptibility; however, structural and functional validation would be necessary to ensure preservation of biological activity. In addition, formulation strategies incorporating hydrotropic agents or surfactants capable of masking hydrophobic surfaces may further enhance stability (Zoeller *et al*., 2022). Stabilization of the C-terminal aggregation-prone segment may also contribute to minimizing aggregation during storage and handling.

Overall, the integration of aggregation scoring, energetic contribution analysis, solvent accessibility assessment, and chain-wise comparison provides a coherent framework for understanding aggregation behavior in BDNF and supports rational approaches for improving its stability as a therapeutic protein. It is important to note that the present findings are derived from computational predictive models and residue-level energetic decomposition. While statistically robust, these results require experimental validation through biophysical aggregation assays, mutational analysis, or structural stability measurements to confirm their functional relevance.

CONCLUSION

The present multi-algorithm computational analysis suggests that aggregation propensity in BDNF is concentrated within specific residue clusters rather than being uniformly distributed across the protein structure. Chain-wise evaluation identified a prominent aggregation-prone segment within residues 60-63 of Chain A, characterized by high aggregation score, elevated hydrophobic energetic contribution, and increased solvent accessibility. Secondary aggregation-prone regions were observed within the C-terminal segment, which may contribute to aggregation progression.

The combined analysis of aggregation scoring, sequence-based prediction, energetic contribution assessment, and solvent accessibility profiling provides a comprehensive understanding of structural regions associated with aggregation susceptibility. These findings may support the rational design of stabilization strategies, including targeted residue modification and formulation approaches aimed at reducing aggregation and improving the stability of BDNF as a therapeutic protein. Future experimental studies will be necessary to validate the mechanistic implications of these computational findings and to confirm the functional relevance of the identified aggregation-prone regions.

ACKNOWLEDGEMENT

We thank PSG College of Pharmacy, Coimbatore, for facilities/support, and The Tamil Nadu Dr. M.G.R. Medical University, Chennai, for academic guidance and affiliation.

ABBREVIATIONS

BDNF: Brain-Derived Neurotrophic Factor; **TrkB:** Tropomyosin Receptor Kinase B; **PDB:** Protein Data Bank; **Å:** Angstrom; **RMSD:** Root Mean Square Deviation; **OPLS4:** Optimized Potentials for Liquid Simulations 4 Force Field; **SASA:** Solvent-Accessible Surface Area; **AggScore:** Aggregation Score; **SD:** Standard Deviation; **π-π:** Pi–Pi Interactions; **a3v:** Aggregation Propensity Scale (Aggrescan intrinsic scale); **kcal/mol:** Kilocalories per mole; **R^2:** Coefficient of Determination; **r:** Pearson Correlation Coefficient; **W:** Shapiro–Wilk Test Statistic; **p:** Probability Value; **Z-score:** Standard Score; **β-sheet:** Beta-sheet Secondary Structure; **GLY:** Glycine; **PRO:** Proline; **MET:** Methionine; **TYR:** Tyrosine; **PHE:** Phenylalanine.

CONFLICT OF INTEREST

The authors declare that there is no conflict of interest.

REFERENCES

Bhachoo, J., and Beuming, T. (2017). Investigating protein-peptide interactions using the Schrödinger computational suite. In *Methods in molecular biology* (pp. 235-254). Humana Press. https://doi.org/10.1007/978-1-4939-6798-8_14

Colucci-D'Amato, L., Speranza, L., and Volpicelli, F. (2020). Neurotrophic factor BDNF, physiological functions and therapeutic potential in depression, neurodegeneration and brain cancer. *International Journal of Molecular Sciences, 21*(20), 7777. https://doi.org/10.3390/ijms21207777

Elhassan, M. S. A., Tran, T. Van, and Lee, C. (2025). Aromatic residue variations in the central β-sheet influence stability and activity of *E. coli* glutaredoxin 3. *ACS Omega, 10*(24), 25810-25818. https://doi.org/10.1021/acsomega.5c01938

Jones, S., and Thornton, J. M. (1997). Analysis of protein-protein interaction sites using surface patches. *Journal of Molecular Biology, 272*(1), 121-132. https://doi.org/10.1006/jmbi.1997.1234

Majid, N., and Khan, R. H. (2023). Protein aggregation: Consequences, mechanism, characterization and inhibitory strategies. *International Journal of Biological Macromolecules, 242*, 125123. https://doi.org/10.1016/j.ijbiomac.2023.125123

Malleshappa Gowder, S., Chatterjee, J., Chaudhuri, T., and Paul, K. (2014). Prediction and analysis of surface hydrophobic residues in tertiary structure of proteins. *The Scientific World Journal, 2014*, 1-7. https://doi.org/10.1155/2014/971258

Navarro, S., and Ventura, S. (2022). Computational methods to predict protein aggregation. *Current Opinion in Structural Biology, 73*, 102343. https://doi.org/10.1016/j.sbi.2022.102343

Pesce, G., Solé, O., Bárcenas, O., and Ventura, S. (2026). AGGRESCAN and its evolution: A two-decade perspective on protein aggregation prediction. *Biophysical Reviews*. Advance online publication. https://doi.org/10.1007/s12551-025-01404-9

Pham, N. B., and Meng, W. S. (2020). Protein aggregation and immunogenicity of biotherapeutics. International Journal of Pharmaceutics, 585, 119523. https://doi.org/10.1016/j.ijpharm.2020.119523

Rabe, M., Verdes, D., and Seeger, S. (2009). Surface-induced spreading phenomenon of protein clusters. *Soft Matter, 5*(5), 1039-1047. https://doi.org/10.1039/b814053g

Rahban, M., Ahmad, F., Piatyszek, M. A., Haertlé, T., Saso, L., and Saboury, A. A. (2023). Stabilization challenges and aggregation in protein-based therapeutics in the pharmaceutical industry. *RSC Advances, 13*(51), 35947-35963. https://doi.org/10.1039/d3ra06476j

Rojekar, S., Gholap, A. D., Jadhav, K., Shevalkar, G., Sugandhi, V. V., Pai, R., Parikh, K., Prajapati, M. K., Desai, N., Vora, L. K., Ingle, R. G., and Paudel, K. R. (2025). Exploring protein aggregation in biological products: From mechanistic understanding to practical solutions. *AAPS PharmSciTech, 26*(6), 189. https://doi.org/10.1208/s12249-025-03189-2

Sankar, K., Krystek, S. R., Carl, S. M., Day, T., and Maier, J. K. X. (2018). AggScore: Prediction of aggregation-prone regions in proteins based on the distribution of surface patches. *Proteins: Structure, Function, and Bioinformatics, 86*(11), 1147-1156. https://doi.org/10.1002/prot.25594

Tartaglia, G. G., and Vendruscolo, M. (2008). The Zyggregator method for predicting protein aggregation propensities. *Chemical Society Reviews, 37*(7), 1395-1401. https://doi.org/10.1039/b706784b

Tien, M. Z., Meyer, A. G., Sydykova, D. K., Spielman, S. J., and Wilke, C. O. (2013). Maximum allowed solvent accessibilities of residues in proteins. *PLoS ONE, 8*(11), e80635. https://doi.org/10.1371/journal.pone.0080635

Zoeller, M. P., Hafiz, S., Marx, A., Erwin, N., Fricker, G., and Carpenter, J. F. (2022). Exploring the protein stabilizing capability of surfactants against agitation stress and the underlying mechanisms. *Journal of Pharmaceutical Sciences, 111*(12), 3261-3274. https://doi.org/10.1016/j.xphs.2022.09.004

Cite this article: Ramanathan M, Nithya R. Computational Identification of Aggregation-Prone Regions in Brain-Derived Neurotrophic Factor (BDNF). J Young Pharm. 2026;18(2):450-6.